JACS
JOURNAL OF THE AMERICAN CHEMICAL SOCIETY

ARTICLE

pubs.acs.org/JACS

pH-Controlled Exponential and Linear Growing Modes of Layer-by-Layer Assemblies of Star Polyelectrolytes

Ikjun Choi,[†] Rattanon Suntivich,[†] Felix A. Plamper,[‡,§] Christopher V. Synatschke,[‡] Axel H. E. Müller,[‡] and Vladimir V. Tsukruk*[,†]

[†]School of Materials Science and Engineering, Georgia Institute of Technology, Atlanta, Georgia 30332-0245, United States

[‡]Makromolekulare Chemie II and Bayreuther Zentrum fur Kolloide und Grenzflächen, Universität Bayreuth, D-95440 Bayreuth, Germany

Supporting Information

ABSTRACT:

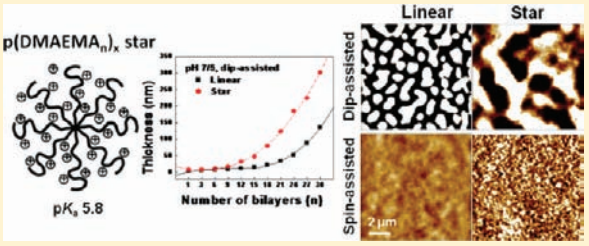

We report the unique layer-by-layer (LbL) assembly behavior of pH-sensitive star-shaped polyelectrolytes with both linear and exponential growth modes controlled by star architecture and assembly conditions. Cationic poly[2-(dimethylamino)ethyl methacrylate] and anionic poly(acrylic acid) stars were synthesized via "core-first" atom-transfer radical polymerization (ATRP) based on multifunctional initiators, in addition to their linear analogues. We demonstrated the LbL growth behavior as a function of deposition pH (ranging from 5 to 7), number of layers (up to 30 bilayers), and the method of assembly (dip- vs spin-assisted LbL). The spin-assisted LbL assembly makes it possible to render smoother and thinner LbL films with parameters controlled by the shear rate and pH conditions. In contrast, for dip-assisted LbL assembly, the pH-dependent exponential growth was observed for both linear and star polyelectrolytes. In the case of linear/linear pair, the exponential buildup was accompanied with a notable surface segregation which resulted in dramatic surface nonuniformity, "wormlike" heterogeneous morphology, and dramatic surface roughening. In contrast, star/linear and star/star LbL films showed very uniform and smooth surface morphology (roughness below 2.0 nm on the scale of 10 μm × 10 μm) with much larger thickness reaching up to 1.0 μm for 30 bilayers and rich optical interference effects. Star polyelectrolytes with partially screened charges and high mobility caused by compact branched architecture appear to facilitate fast diffusion and exponential buildup of LbL films. We suggest that the fast buildup prevents long-range lateral diffusion of polyelectrolyte star components, hinders large-scale microphase separation, and thus leads to unique thick, smooth, uniform, transparent, and colorful LbL films from star polyelectrolytes in contrast to mostly heterogeneous films from traditional linear counterparts.

INTRODUCTION

Layer-by-Layer (LbL) multilayer assembly[1−4] is an intriguing subject of continuous interest because it can offer a variety of functional organized nanomaterials for various applications.[5−17] The LbL assembly consists of successively adsorbed macromolecular or nanoparticulate layers bonded via electrostatic interaction,[1] hydrogen bonding,[18] and hydrophobic interaction[19] by controlling various parameters such as pH, ionic strength, temperature, and concentration, which affect the integrity and strength of LbL films.[2,7,20,21] Recently, much effort has been made to design weakly bonded stimuli-responsive thin films and microcapsules from LbL multilayer assemblies.[22−27] In particular, the LbL multilayer assemblies based on weak polyelectrolytes such as poly(acrylic acid) (p(AA)), poly(allylamine hydrochloride) (p(AH)), or poly(methacrylic acid) (p(MAA)) exhibit various pH-responsive behaviors, which can be tuned by the adjustment of the ionic strength and charge density of the polyelectrolytes, as well as environmental conditions such as pH, salinity, and multivalent counterions.[28−30] Due to pH-triggered volume phase transformations (i.e., "coil to globular" chain conformational transition), weak polyelectrolytes have been recognized as a promising building component for the effective manipulation of the chemical and structural properties of LbL assemblies.[22,31,32] However, the LbL multilayer growth mechanism in exponential mode has not been completely understood yet, especially for complex polyelectrolyte architectures such as star polyelectrolytes.

Received: April 5, 2011
Published: May 18, 2011

dx.doi.org/10.1021/ja203106c | J. Am. Chem. Soc. 2011, 133, 9592–9606

Recent advancements in controlled/living polymerization methods, especially atom-transfer radical polymerization (ATRP), allow for intense research on branched polymers with novel architectures such as star-shaped block copolymers and polyelectrolytes.[33−39] The architecture of such branched polymers features compact, globular chain conformation and multiple chain ends. This molecular structure leads to diverse physical and chemical properties in bulk, in solution, and at interfaces due to the reduced hydrodynamic volume compared to the linear counterpart with an equivalent molecular weight. For instance, it has been observed that amphiphilic branched block copolymers exhibit peculiar surface morphologies of their thin films at the interface.[40−44] In particular, pH-sensitive star-shaped polyelectrolytes and dendrimers are considered to be an intriguing component for LbL films because of their unique chemical properties such as high charge density and multiple reactive sites of terminal groups.[45−47] Interestingly, the highly branched polyamidoamine (PAMAM) dendrimer was found to interdiffuse in multilayers at lower critical degree of ionization (55%).[48,49] In addition, weak star polyelectrolytes exhibit a distinct shift of pK_a value as compared to linear ones.[50,51] This phenomenon is caused by an ionic confinement effect due to the highly crowded chain structure of star polymers because of the increased osmotic pressure inside star polymers.[35]

Apart from the properties of polyelectrolytes such as ionic strength, charge density, and molecular weight and structure, assembly techniques such as dip-,[5] spray-,[52] or spin-assisted[53−56] methods play a critical role in determining the mode of growth, intermixing state, and final morphology and physical properties of LbL films as controlled by the balance of adsorption, diffusion, the presence of nanostructures, and the degree of hydration.[57−67] A recent comparative study of spray- and dip-assisted methods has shown that a spray-assisted LbL allows thinner, less dense, and rougher films than a dip-assisted method.[68] Spin-assisted LbL assembly rapidly provides highly mechanically robust and stratified LbL films by controlling shear force and solvent evaporation.[53,69,70] The shear effect can promote mass transfer enhancing intermolecular interaction as well as prevent interlayer mixing due to the limited diffusion by quick solvent removal.[53,54,71] To date, however, it is not clear how different LbL assembling approaches can allow for growing much thicker (micrometers) films by utilizing an exponential mode of LbL growth.

Indeed, since the first report of the exponential growth of polylysine and polyalginate,[72−75] both regular (linear) and exponential (nonlinear) growing modes were observed for LbL films from a variety of linear polyelectrolytes. As is known, the exponential growth of LbL films can be caused by the increasing roughness of adsorbed polyelectrolytes with low charge density which undergo surface-assisted microphase separation as well as excessive adsorption of components facilitated by the "in-and-out" diffusion of polymer chains. Specifically, weakly bonded free polymer chains diffuse across the hydrated swollen film during endothermic complexation in the course of the adsorption process. Recently, a three-zone model was suggested and "exponential-to-linear" transition in LbL assembly was experimentally demonstrated and discussed.[76,60] Also, the interdiffusion and dynamic exchange of weak polycations within LbL multilayers was found to occur at a critical ionization of around 70% for different chain topologies (linear, branched, and dendrimer).

Despite the intriguing architecture of star polyelectrolytes, they have rarely been explored for building LbL assemblies because of their complex interfacial behavior. Recently, Yang et al. discussed composite thin films composed of a star-shaped poly(acrylic acid) (p(AA)) polymer brush having a poly(methylsilsesquioxane) (PSQ) core with poly(vinylpyrrolidone) (p(VPON) via hydrogen bonding interactions.[77] Thin films showing reversible morphological transitions that were assembled from pH-responsive star p(AA) and linear p(AH) were explored by Connal et al.[78] Distinct morphological changes under post-pH treatment were also observed by Kim et al. in LbL films from star-shaped and pH responsive poly[2-(dimethylamino)ethyl methacrylate] (p(DMAEMA)) and p(AA).[79] They proposed the unique compact structure of the star polymer and a resulting limited interpenetration of the polymers to be responsible for those changes. A recent study by Guo et al. demonstrated that LbL films of star p(DMAEMA)/poly(sodium 4-styrenesulfonate) (p(SS)) showed exponential growth as a function of arm length and number of arms.[80] Still, no systematic study on the modes of growth of star polyelectrolytes has been conducted to date. It is unclear how the incorporation of star polyelectrolytes can facilitate a fast exponential mode of LbL growth and provide for responsive properties and if the mode of LbL growth can be tuned with pH control during assembling process.

Here, we report pH-tunable LbL growth modes of pH-sensitive stars; p(DMAEMA) with variable molecular weights and number of arms, which are consecutively deposited with p(AA) stars; and corresponding linear counterparts at varying pH conditions. To understand the effect of ionic states on LbL assembly, both dip-assisted and spin-assisted LbL assemblies were explored to build LbL films with the number of bilayers reaching 30 at various pH (from pH 5 to 7). Moreover, different pairs of combinations including linear−star, star−linear, and star−star were also used to understand the role of molecular architecture on the LbL assembly. We suggest that in the exponential mode fast buildup prevents long-range lateral diffusion of polyelectrolyte star components which hinders microphase separation and leads to thick, smooth, uniform, transparent, and colorful films from star polyelectrolytes in contrast to traditional linear counterparts.

In this paper, we demonstrate the pH-tunable exponential/linear growth behavior of star polyelectrolytes in the course of LbL assembly. We found a distinct evolution of surface morphology of star polyelectrolytes during LbL buildup which is different from that known for linear counterparts. The fast exponential growth observed at certain assembly conditions suggests that the vertical diffusion of star polyelectrolytes within LbL films occurs efficiently in spite of their large molecular weights. We suggest that globular and compact molecular conformations play a pivotal role in facilitating high mobility and interdiffusion needed for exponential mode of growth. The LbL assembly conditions are systematically explored for various combinations such as linear/linear, linear/star, star/linear, and star/star polyelectrolyte pairs. These efforts clearly reveal that both linear and exponential growth modes result in LbL films with varying thicknesses and morphologies. The growth modes can be finely tuned with pH conditions which in turn affect the interplay of various parameters such as charge density, degree of hydration, and molecular diffusion, discussed as followso.

EXPERIMENTAL SECTION

Materials. Linear p(AA_{1400}) (M_W = 100 kDa), p(SS_{380}) (M_W = 70 kDa), and p(AH_{600}) (M_W = 56 kDa) (the index indicating the degree of polymerization) were obtained from Aldrich and were used as-received. 1.0 M Tris HCl was purchased from Rockland and was diluted

dx.doi.org/10.1021/ja203106c |J. Am. Chem. Soc. 2011, 133, 9592–9606

Table 1. Molecular Characteristics of Polyelectrolyte Components for LbL films

entry	formula	initiator	PDI[a]	$M_{n,star} \times 10^{-3}$ [b] (g/mol)	$M_{n,arm} \times 10^{-3}$ [c] (g/mol)	pK_a [d]
1	$p(AH_{600})$	commercial		56		
2	$p(DMAEMA_{880})$	EBIB	1.9	139		6.2
3	$p(DMAEMA_{170})_{5.6}$	saccharose[50]	1.2	146	27	6.0
4	$p(DMAEMA_{170})_{18}$	silsesquioxane[50]	1.4	490	27	5.8
5	$p(SS_{320})$	commercial		70		
6	$p(AA_{1400})$	commercial	~1.1	100		6.2
7	$p(AA_{125})_{21}$	cyclodextrin[23]	1.1	190	9	6.7

[a] Calculated from the NMR conversion data together with the initiator concentration. [b] Determined by GPC in THF (containing 0.25 wt % TBAB for cationic polyelectrolytes) and polystyrene standards. [c] Calculated by dividing the total molecular weight of star by the number of arms. [d] Apparent value measured as pH at degree of neutralization $\alpha = 0.5$, 1 g/L in pure water.[35]

to 0.01 M in Nanopure water for use. Solutions of 0.1 M HCl (99.5% purity) and 0.1 M NaOH (99.5%) were utilized to adjust the pH of polyelectrolyte solutions.

Synthesis of the Star and Linear Polyelectrolytes. In short, star-shaped p(DMAEMA) and p(AA) were synthesized by ATRP in a core-first approach.[81,35,50] As multifunctional initiators either saccharose-, cyclodextrin-, or silsesquioxane-based cores functionalized with 2-bromoisobutyryl groups were used. The detailed synthesis and characterization of these initiator molecules is given in the above references. For the linear polymers we used ethyl 2-bromoisobutyrate (EBIB) as the initiator. The number of arms was determined by cleaving off the arms from the core.[35] The molecular characterization of the polymers is summarized in Table 1, where the subscripts n and x of the formula $p(NAME_n)_x$ denote the average degree of polymerization of each arm and the number of arms, respectively.

Preparation of LbL Multilayer Assemblies. Polyelectrolytes were dissolved in Nanopure water (18.2 MΩ cm) or in 0.01 M Tris HCl buffer solution. p(AH) and p(SS) amounts of 0.2 wt % (2.0 mg/mL) were used for the precursor layer by the deposition of 2.5 bilayers of $(PAH/PSS)_{2.5}$ to improve the initial adhesion and to obtain the same initial condition prior to the assembly of the main p(AA) and p(DMAEMA) LbL multilayer film. Polyelectrolyte solutions of p(AA) and p(DMAEMA) were prepared to 0.02 wt % (0.2 mg/mL) in concentration with 0.01 M Tris HCl buffer solution. The pH of all the solutions was adjusted by the addition of 0.1 M HCl or 0.1 M NaOH aqueous solution to control the charge density of polyelectrolytes.

Freshly cut silicon substrates with dimensions of 1 cm × 2 cm and the [100] orientation (semiconductor processing) and a native silicon oxide layer were cleaned with piranha solution (3:1 concentrated sulfuric acid and hydrogen peroxide mixture. *Caution strong oxidizer!*) in accordance with the usual procedure.[82,83] Subsequently, it was abundantly rinsed with Nanopure water and dried with a dry nitrogen stream. Pretreated fresh wafers served as hydrophilic substrates for LbL film deposition.

Spin-assisted LbL films were prepared by using sequential spin-casting at different revolutions per minute (rpm) for 20 s and rinsed twice between depositions of polyelectrolyte solution under the same condition in accordance with the usual procedure in our laboratory.[84,85] Subsequently, LbL films were spun for 1 min to remove water under dry nitrogen and further dried at room temperature for 48 h before experimental measurements. The p(AA) and p(DMAEMA) layers were deposited alternately up to 30 bilayers. The dip-assisted LbL process was performed by alternate immersion of the substrates in polyelectrolyte solutions for 10 min, followed by rinsing three times with the same pH buffer solution.

Characterization of LbL Films. Measurement of the film thicknesses and refractive indices were carried out with a Woollam M2000U (J. A. Woollam Co., Inc., Lincoln, NE) multiangle spectroscopic ellipsometer with a WVASE32 analysis software for three incident angles 65, 70, and 75°. The Ψ (polarized angle) and Δ (phase) values were measured and used to construct a Cauchy model to determine the optical constants n and k over wavelengths of 245−1000 nm (Figure S1). These data were used to determine the thickness of the LbL films by fitting the data to the Cauchy approximation using a multilayer structure model composed of silicon, silicon oxide, and the LbL film of interest. The thickness of silicon and silicon oxide ($n = 1.46$; native thickness, 2.0 nm) was determined prior to deposition of polyelectrolyte LbL film from the well-known reflective index. The LbL film thickness data were fit to the Cauchy model where the reflective index is given as $n(\lambda) = A_n + B_n/\lambda^2 + C_n/\lambda^4$ with $A_n = 1.45$, $B_n = 0.01$, and $C_n = 0.0$ as a function of λ. For sufficiently thick films, thickness was determined using fitted Cauchy constants obtained from Ψ and Δ of measured films. The mean squared error (MSE) for data fitting was in the range of 5−25. Thickness measurements were conducted on at least three different homogeneous surfaces for each sample showing standard deviation within ±8% level.

Atomic force microscopy (AFM) images were obtained with a Dimension-3000 in the "light" tapping mode with an amplitude ratio, within 0.90−0.99 to avoid surface damage and film deformation.[86,87] The AFM cantilevers had spring constants in the range of 40−60 N/m. Scanning rates were between 1.0 and 2.0 Hz, depending on the scan area that ranged from 40 × 40 μm^2 down to 1 × 1 μm^2.[88] The large area optical microscope images were collected by optical microscopy operating in the bright field mode (Leica DM4000M). UV−vis spectroscopy was conducted on a Craic QDI 202 microscope spectrophotometer attached to a Leica microscope with a 50× objective. Measurement of contact angles were undertaken with a KSV CAM101 at three different locations for each sample.

RESULTS AND DISCUSSION

LbL Assembly from Star and Linear Polymers at Variable pH. pH-sensitive p(DMAEMA) and p(AA) polymers are weak polyelectrolytes which can be ionized depending on pH with respect to the pK_a of p(DMAEMA) and p(AA) (Table 1, Scheme 1). The apparent value of pK_a is defined as the pH when 50% neutralization of total ionic monomer units occurs in a titration curve. The pK_a shift of polyelectrolyte star compared to the linear polymer has been known to be caused by the increased confinement of counterions within the macroion.[78,89] This results in a higher osmotic pressure within the star polymers which constrains the neutralization. The shifts are dependent on not only the degree of neutralization but also the number of arms and arm length due to the variation of mean segment density within the star.[35,50] The pH-dependence of weak polyelectrolytes has a significant influence on the molecular conformation in solution and at the interface by undergoing the "coil-to-globule" phase transitions.[90] Cationic p(DMAEMA) stars having a

Scheme 1. pH-Responsive Molecular Conformation of (a) Cationic $p(DMAEMA_n)_x$ and (b) Anionic $p(AA_n)_x$ Star Polyelectrolyte with the Chemical Structure of Monomer Unit of Star Polyelectrolyte[a]

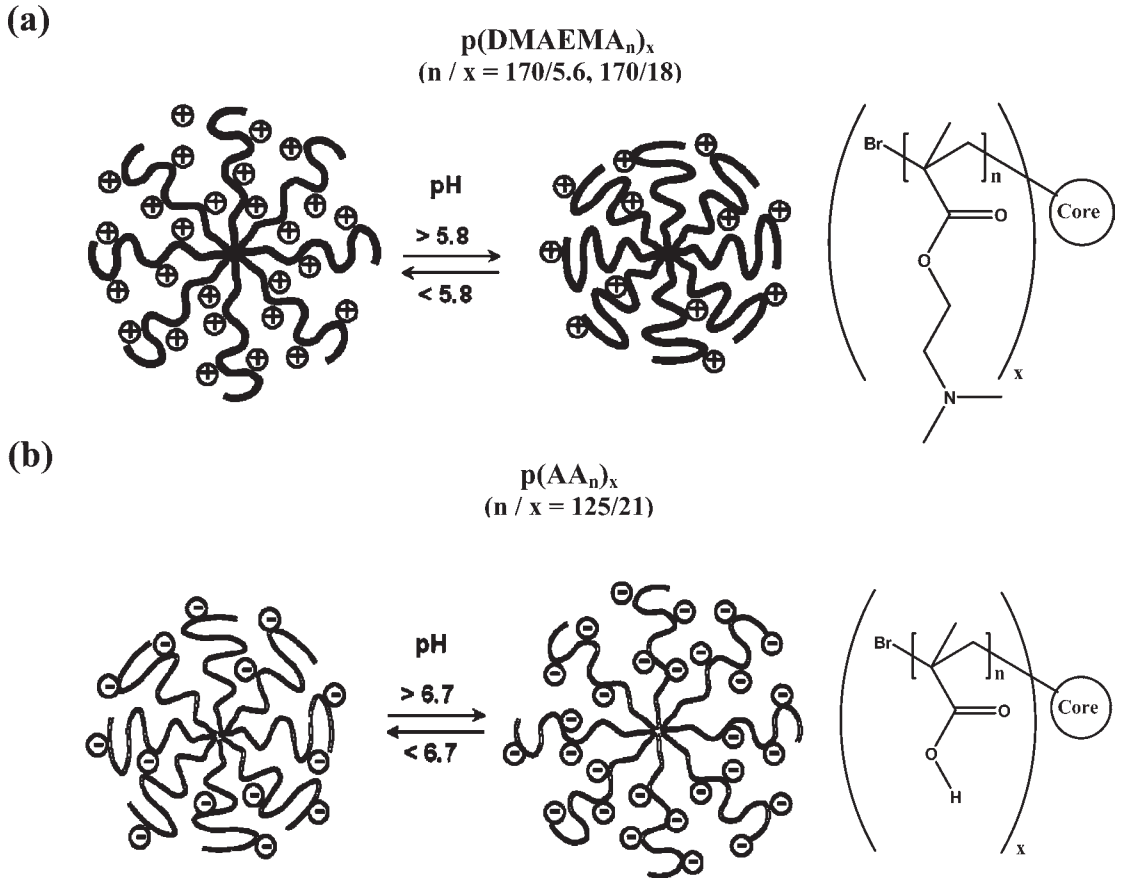

[a] *n* refers to the degree of polymerization of each arm, and *x* denotes the number of arms. It is not set to the real length-scale for all drawings.

Table 2. Polymer Pair and Notation of p(AA) and p(DMAEMA) for LbL Assemblies

polymer pair		DP[a] of arm (*n*)/no. of arms (*x*)		molecular weight ($\times 10^{-3}$ g/mol)
p(AA)/p(DMAEMA)	notation	$p(AA_n)_x$	$p(DMAEMA_n)_x$	$M_{n,p(AA)}/M_{n,p(DMAEMA)}$
linear/linear	LL	1400/1	880/1	100/139
linear/star	LS	1400/1	170/5.6	100/146
star/linear	SL	125/21	880/1	190/139
star/star	SS	125/21	170/18	190/490

[a] DP refers to the degree of polymerization.

different number of arms (5.6 and 18) with the same degree of polymerization of each arm employed to evaluate the effect of the number of arms (see characteristics of all components in Table 1).

Then, we chose and compared different polymer pairs to assemble LbL films based on star (S) or linear (L) p(DMAEMA) and p(AA) polyelectrolytes (Table 2). Four different pairs were selected for LbL assembly to represent components with different numbers of arms and degrees of polymerization of each arm (Scheme 1). For convenience, the same notation (LL, SL, LS, and SS, see Table 2) referring to each LbL pair will be utilized throughout this paper. A bilayer is defined as a polyelectrolyte pair composed of one polyanionic p(AA) layer and one polycationic p(DMAEMA) layer. Two and a half (2.5) bilayers of $(p(AH)/p(SS))_{2.5}$ with p(AH) as the topmost layer were employed to improve the initial adhesion and provide the same initial condition prior to assembling the main p(AA) and p(DMAEMA) LbL multilayer film.

Both spin-assisted and dip-assisted LbL methods were employed at various assembly pH conditions such as pH 5/5, 5/7, 6/5, 6/6, 7/5, and 7/7 to explore the pH-sensitive assembly behavior of weak linear/star polyelectrolytes. In this pH notation the first figure refers to the solution pH of the p(AA) component and the second one is the pH of the p(DMAEMA) solution. The region ranging from pH 5 to 7 is chosen here because it covers the pK_a of both p(DMAEMA) and p(AA) that are considered to give

dx.doi.org/10.1021/ja203106c |*J. Am. Chem. Soc.* 2011, 133, 9592–9606

different interactions between polymer pairs (Table 1) and ensures stable LbL growth. We also explored more acidic (down to pH 2) and basic (up to pH 8) conditions. However, these conditions led to extremely nonuniform and unstable films and thus were not studied in detail further.

In the selected region ranging from pH 5 to 7, the variation of the LbL film thickness shows a high dependency on the dipping solution pH condition (Figure 1). A lower pH than 5 for p(AA) and a higher pH than 7 for p(DMAEMA) appear to induce the desorption of the LbL film during the spin-assisted LbL assembly due to insufficient ionic charge density as will be discussed later. Considering the pK_a values of both components are within 5.8−6.7, the pH combinations represent pairs with the weakest electrostatic interactions (pH 5/5, 6/6, and 7/7) in contrast to pairs with the strongest interactions of components at pH 7/5 and 7/6. Moreover, the expectation is that p(AA) is in a compact shape and p(DMAEMA) is in an expanded state for lower pH (5 and 6) and vice versa for higher pH (7) although variation of molecular dimensions of the star components is much less pronounced than that for the linear counterparts.[78,79,35]

For the linear p(AA) and star p(DMAEMA) pair (LS, Table 2), we examined the spin-assisted LbL growth at variable pH conditions by measuring the thickness of LbL films with an increasing number of bilayers (Figure 1a). The results revealed that the LbL assembly behavior appears to be close to the linear buildup profile in all cases.

It is clear that the growth of LbL films depends upon the assembly pH conditions: at pH 7/5 and 5/7, the resulting thickness observed was the lowest while at pH 5/5 and 6/6, the thickest LbL films were shown (Figure 1, Supporting Information Table S1). Thickness variations are similar for 6 and 18 bilayer films within 50−100% variation for thin films which increases to 200−300% for thicker LbL films (18 bilayers) (Figure 1).

AFM topography images of these films, presented in Figure 2 (see Supporting Information Figures S2 and S3 for 6 bilayers), show clear differences in surface morphologies at different pH at both large and fine scales. A smooth morphology was observed for all specimens except LbL films assembled at pH 5/7 conditions. Indeed, surface roughness was within 0.2−1.7 nm at a 20 μm × 20 μm surface area with higher values for modestly phase separated films at pH 6/6 and 7/6 (Table S1). Surface roughness below 0.5 nm for 1 μm × 1 μm surface area is also characteristic of uniform, molecularly smooth LbL films grown in a linear regime (Figure 1c, Table S1). The formation of polyelectrolyte complexes in most of the cases would lead to a smooth surface due to a "ladderlike" architecture with a stretched conformation, whereas partially ionized chains can adopt a "scrambled salt conformation" composed of a high percentage of "loops" and "tails" which results in odd surface morphology.[7]

In the case of pH 5/5, the LbL film thickness is the highest, but the surface appears to be very even showing a smooth morphology as compared to that of pH 5/7 (Figure 2, Supporting Information Figure S3). This result indicates that at lower pH conditions more ionized arms of p(DMAEMA) should form a smooth surface by adopting a stretched conformation.[91,92] In contrast, AFM images of pH 5/7 LbL films show very uneven surface morphology with surface corrugation at micrometer and submicrometer scales and developed surface roughness as high as 4.7 nm at large surface areas (20 μm × 20 μm) and 2.3 nm for fine surface areas (1 μm × 1 μm) (Figure 1c).

This uneven surface morphology can be an indication that a stable complexation cannot be successfully realized due to the weak electrostatic interactions at this pH condition.[91,92] Indeed, both p(AA) and p(DMAEMA) components are weakly charged under these conditions with the collapsed state of linear p(AA) further promoting local phase separation. The overall trends in thickness and roughness variation are similar for 6 and 18 bilayer LbL films with more pronounced roughening visible for pH 5/5 LbL films (Figure 2).

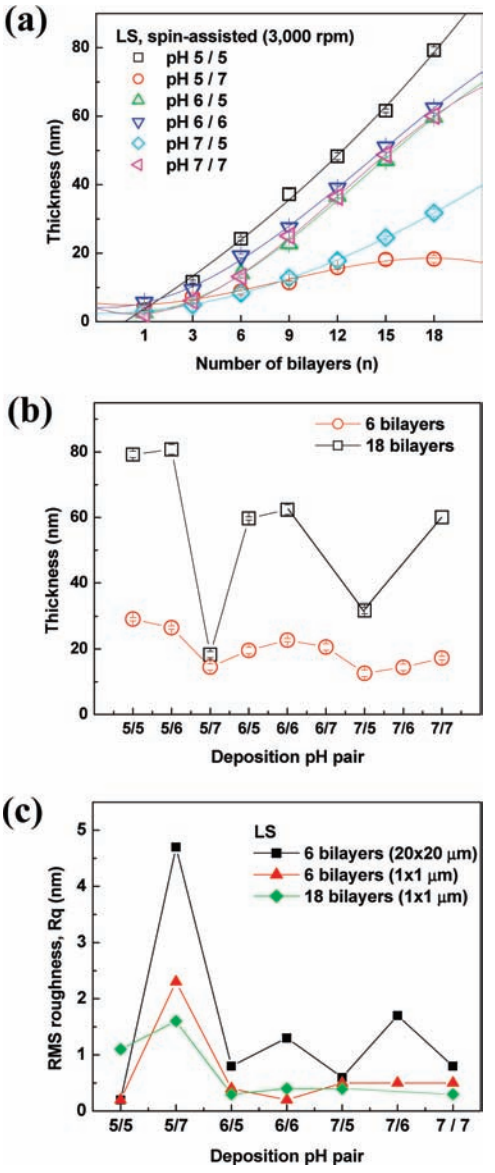

Figure 1. (a) Buildup curve of linear/star (LS) film versus the number of bilayers prepared using spin-assisted method (3000 rpm) at various combinations of deposition pH conditions for p(AA)/p(DMAEMA) pairs: pH 5/5, 5/7, 6/7, 6/6, 7/5, and 7/7. (b) Variations of thickness of LS for 6 bilayers and for 18 bilayers versus different deposition pH pairs. (c) Root mean square (RMS) roughness for LS at different scan areas and number of bilayers: 20 μm × 20 μm of 6 bilayers (■), 1 μm × 1 μm of 6 bilayers (▲), and 1 μm × 1 μm of 18 bilayers (♦) (the lines are a guide to the eye).

Spin-Assisted vs Conventional LbL Assembly: Different Modes of Growth. The different LbL assembly methods are known to define the morphology of LbL films due to distinct mass flow, drying rate, and diffusion characteristics.[53,99] To

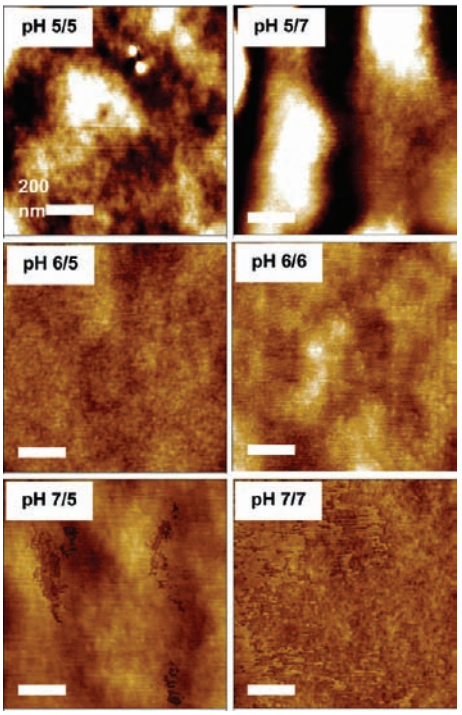

Figure 2. AFM topography images of linear/star LbL films (LS) with 18 bilayers assembled by using spin-assisted method at different pH pairs. The scan area for all images is 1 μm × 1 μm, and the Z scale is 5 nm.

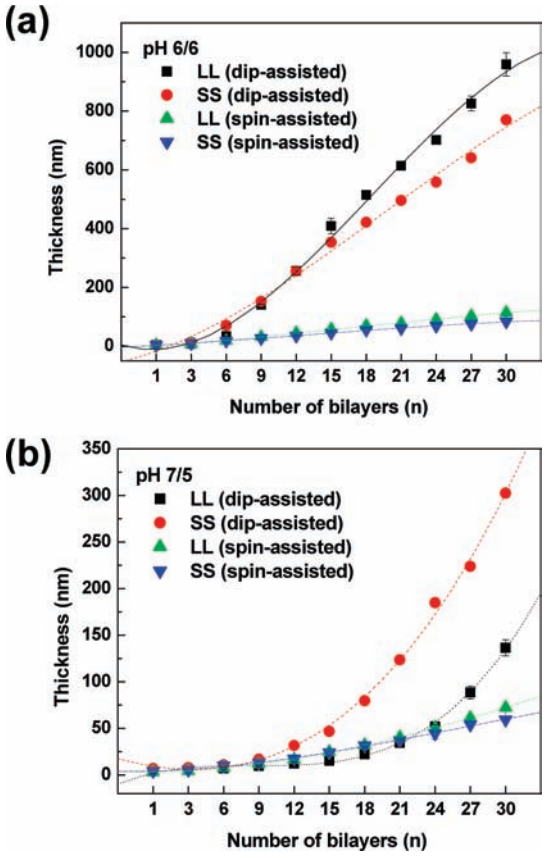

Figure 3. Buildup curve of the LbL multilayer assembly of varying combinations of linear and star polyelectrolytes as a function of number of bilayers (1−30 bilayers) at different pH conditions of (a) pH 6/6 and (b) pH 7/5: LL (dip-assisted (■) and spin-assisted (▲)) and SS (dip-assisted (●) and spin-assisted (▼)) (the lines are a guide to the eye).

investigate this aspect, we selected two different assembly pH conditions which generated the highest adsorbed amount at pH 6/6 and the lowest growth rate at pH 7/5. Under these conditions, the growth curve of linear- and star-based LbL multilayers was examined for up to 30 deposited bilayers (60 deposition cycles; Figure 3).

The linear growth of spin-assisted LbL films at pH 6/6 showed a low increment of 3.8 nm/bilayer for the linear/linear pair and an even lower, 2.8 nm, increment for the star/star pair (Table 3, Figure 3). The thicknesses of 30 bilayers, 117 nm for linear/linear film and 92 nm for star/star film, determined from ellipsometry and from AFM scratch tests are virtually identical, indicating the uniformity of the films. The same trend is observed for pH 7/5 deposition conditions with the growth increment further decreasing to 2.0 nm/bilayer for the linear/linear pair and to 2.4 nm for the star/star pair (Figure 3).

For linear/linear pairs (pH 6/6 and 7/5) prepared by the dip-assisted method, the increased surface roughness (roughness up to 50 nm for 30 bilayers) of LbL film with increasing numbers of bilayers was observed to reduce reflectivity of the film due to light scattering. However, the intensity of reflected light was sufficiently high for determining the film thickness (raw data of Ψ and Δ are presented in Figure S1), indicating the LbL films remain optically transparent and uniform despite increased surface roughness.

Since the ellipsometry measurement gives a relative thickness value, AFM height analysis was used to confirm the thickness of the LbL film. The thickness from ellipsometry was in agreement with the thickness obtained from the height difference seen between bare silicon and the top of the film during an AFM scratch test.[7,26,93,94] This result clearly showed that the increased surface roughness (up to 50 nm) has no significant effect on the accuracy of the thickness measurement by ellipsometry due to the fact that the total thickness of LbL films is much (around 10-fold) higher than the surface inhomogeneities. However, the error in thickness measurement tends to be increased with an increase in thickness and surface roughness.

In contrast, the LbL films obtained by the dip-assisted method grow at a much higher rate (Figure 3). At pH 6/6 the initial exponential growth for a number of bilayers 3−12 is replaced with a linear growth with a high increment of around 30 nm/bilayer. A similar trend is observed for both linear/linear and star/star pair LbL assemblies obtained with the dip-assisted method. The overall LbL thickness approached 1 μm for only 30 bilayers (Table 3).

Remarkably, under different assembly conditions, at pH 7/5 we observed exponential growth for both linear/linear and star/star LbL assemblies with the number of bilayers above 9 (Figure 3). In this mode, the rate of growth is the highest at the latest stage of growth, reaching 50 nm/bilayer for n = 20−30 and far exceeding the average increment of around 30 nm for dip-assisted pH 6/6 LbL films and around 3 nm for spin-assisted LbL films (Figure 3). To further explore the evolution of the surface morphology of LbL growth behavior, AFM images were compared for the different number of bilayers (9, 18, 30) for pH 6/6 and 7/5 (Figures 4 and 5). As presented in Figures 4B,C and 5C, a distinct large surface domain morphology (domain height reaching 150 nm) was observed at both pH 6/6 and 7/5.

dx.doi.org/10.1021/ja203106c |J. Am. Chem. Soc. 2011, 133, 9592–9606

Table 3. Thickness and Roughness of Spin- and Dip-Assisted LbL Films

			thickness (nm)					rms roughness[d] (nm)		
pH	method	polymer pair	$n = 9$ [a]	$n = 18$ [a]	$n = 30$ [a]	$n = 30$ [b]	$n = 30$ [c]	$n = 9$	$n = 18$	$n = 30$
6/6	dip	LL	141.3 ± 0.5	514.6 ± 15.0	959.1 ± 39.7	1032.5 ± 8.0	790	2.9	29.7	49.8
		SS	152.6 ± 2.0	422.0 ± 2.0	770.4 ± 10.9	797.6 ± 3.0	757	2.1	3	1.7
	spin	LL	31.6 ± 1.5	70.0 ± 1.0	114.5 ± 0.3	117.0 ± 4.0	–	0.5	0.6	0.7
		SS	26.7 ± 1.0	56.0 ± 2.0	83.7 ± 3.0	92.0 ± 7.0	–	0.8	1.1	1.7
7/5	dip	LL	9.7 ± 1.0	22.1 ± 3.0	136.4 ± 8.5	144.9 ± 6.0	–	0.6	0.9	46.0
		SS	16.8 ± 2.0	79.6 ± 1.0	302.5 ± 5.0	307.5 ± 2.0	–	1.7	3.4	6.7
	spin	LL	13.1 ± 2.0	31.5 ± 0.1	59.3 ± 3.0	60.2 ± 2.0	–	0.4	0.8	0.6
		SS	11.8 ± 0.7	32.1 ± 0.6	72.4 ± 2.0	80.5 ± 4.0	–	0.5	0.8	1.7

[a] Obtained by fitting the ellipsometry data to the Cauchy model. [b] Measured using a scratching method by AFM height analysis. [c] Thickness values were obtained from UV−vis interference fringe data by plotting $l/2$ vs n/λ using the equation of $l/2 = 2d(n/\lambda)$, where $l/2$ is the interference order; d, the thickness; n, the refractive index; and λ, the wavelength.[96] [d] All rms roughness values were collected from the AFM image of 10 μm × 10 μm.

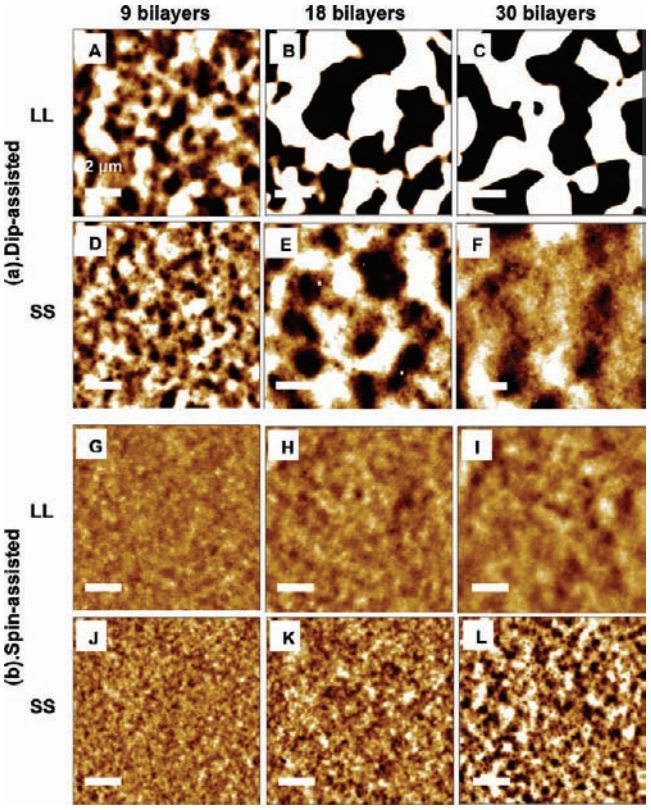

Figure 4. AFM topography images of the LbL multilayer films composed of different components with different numbers of bilayers (9, 18, and 30 bilayers): LL (A−C, G−I) and SS (D−F, J−L) assembled at pH 6/6 using dip-assisted (a) (A−F) and spin-assisted (b) (G−L) methods. The scale bar is 2 μm, and Z scale is 10 nm for all images.

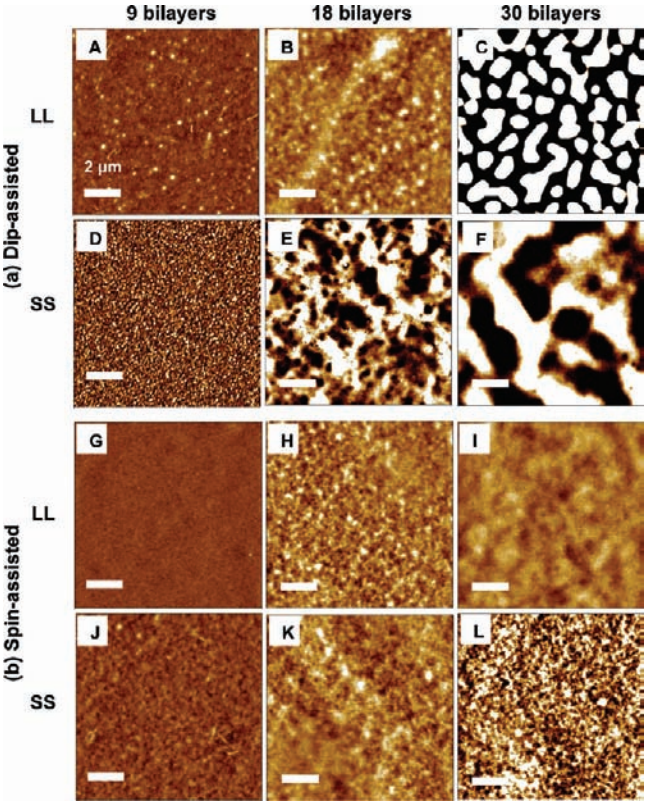

Figure 5. AFM topography images of the LbL multilayer films composed of different components with different numbers of bilayers (9, 18, and 30 bilayers): LL (A−C, G−I) and SS (D−F, J−L) assembled at pH 7/5 using dip-assisted (a) (A−F) and spin-assisted (b) (G−L) methods. The scale bar is 2 μm, and Z scale is 10 nm for all images.

The distinct surface corrugation appears to occur at microscopic length scales throughout the samples. The surface roughness on the scale of 10 μm × 10 μm increases with increasing number of bilayers (Table 3). We note that at pH 6/6 and pH 7/5 linear/linear LbL films display a rougher surface than star/star for the dip-assisted method in contrast to the results of the spin-assisted LbL which showed the opposite trend (Figures 4 and 5). Star/star spin-assisted LbL films show significant increase in roughness on the scale of 10 μm × 10 μm compared to linear/linear counterpart. Overall, spin-assisted LbL films show smoother morphology and lower roughness on the 10 μm × 10 μm scale than dip-assisted films for all combinations studied here.

This difference suggests that star polymers with large molecular weight can be distributed unevenly and accumulate as larger aggregates due to progressing phase separation with an increasing number of bilayers deposited and time available for diffusion and rearrangement (hours) although the shear force and short processing times of the spin-assisted method make them

transform into a smooth morphology with very fine roughness on the 10 μm × 10 μm scale. It appears that, for the linear/linear pairs, the spin-assisted LbL method prevents intermixing within the multilayers due to limited diffusion time induced by the quick solvent removal. In contrast, for the case of the star/star pairs, shearing is believed to allow transformation of spherical star polyelectrolyte macromolecules into a flattened pancakelike shape.[99]

Contact angle measurements were further performed to monitor the change in surface wettability of LbL films with a topmost layer of p(DMAEMA (Supporting Information Figure S4). Overall, a contact angle within 50−70° indicated a modestly hydrophobic surface which is within the range reported for ultrathin surface layers of the p(DMAEMA) component (65°).[95] Some modest variation for different LbL films can be related to variable surface roughness, drying conditions, and minor exposure of the underlying, hydrophilic p(AA) component with an effective contact angle below 10°.[91,92] Thicker 30 bilayer films demonstrate more uniform values of contact angles across all LbL films with different compositions. For LbL films at pH 6/6 with 30 bilayers we observed a slightly lower contact angle of 57 ± 3° than 63 ± 3° for pH 7/5 LbL films, which can be related to a more collapsed topmost layer of p(DMAEMA) due to the surface diffusion of the p(AA) layer (Figure S4).

Optical Properties of LbL Films. Optical microscopy images of the 30 bilayer linear/linear dip-assisted LbL films show large-scale nonuniform patterns of different intensity in contrast to the uniform spin-assisted LbL films (Supporting Information Figure S5). This surface inhomogeneity is indicative of the occurrence of dramatic phase changes caused by phase separation during the assembly process. A more notable rough surface was observed for linear−linear pairs fabricated by the dip-assisted method confirming the AFM data discussed above. Star/star pairing resulted in much more uniform films on an optical scale (Figure S5).

As a result of the overall uniformity, linear and star LbL films display sharp and rich color variation with an increase in thickness due to interference phenomena for sub-micrometer films. For pH 6/6 and pH 7/5 the reflective star/star LbL films obtained with the dip-assisted method give a microscopically uneven surface with multiple colors of green and violet. Linear/linear LbL films look less reflective, which can be ascribed to their higher film inhomogeneities in the optical range (Figure S5). Spin-assisted LbL films with smaller thicknesses showed a relatively uniform bluish color for both linear and star components. LbL films at pH 7/5 showed similar results for the different assembly methods and pH conditions, but the overall color appearance is not well developed due to the smaller thickness of the LbL films.

The UV−vis measurements, which were utilized to quantify the rich color appearance, clearly display a broad peak or a series of periodic peaks related to the light interference for thicker LbL films of linear/linear and star/star LbL films fabricated by the dip-assisted method at pH 6/6 (Figure 6). Multiple interference peaks with several harmonics is a peculiar feature of these films with thicknesses close to 1000 nm that suggests that the LbL films remain optically clear and uniform at the micrometer scale despite the high level of surface corrugation observed with optical

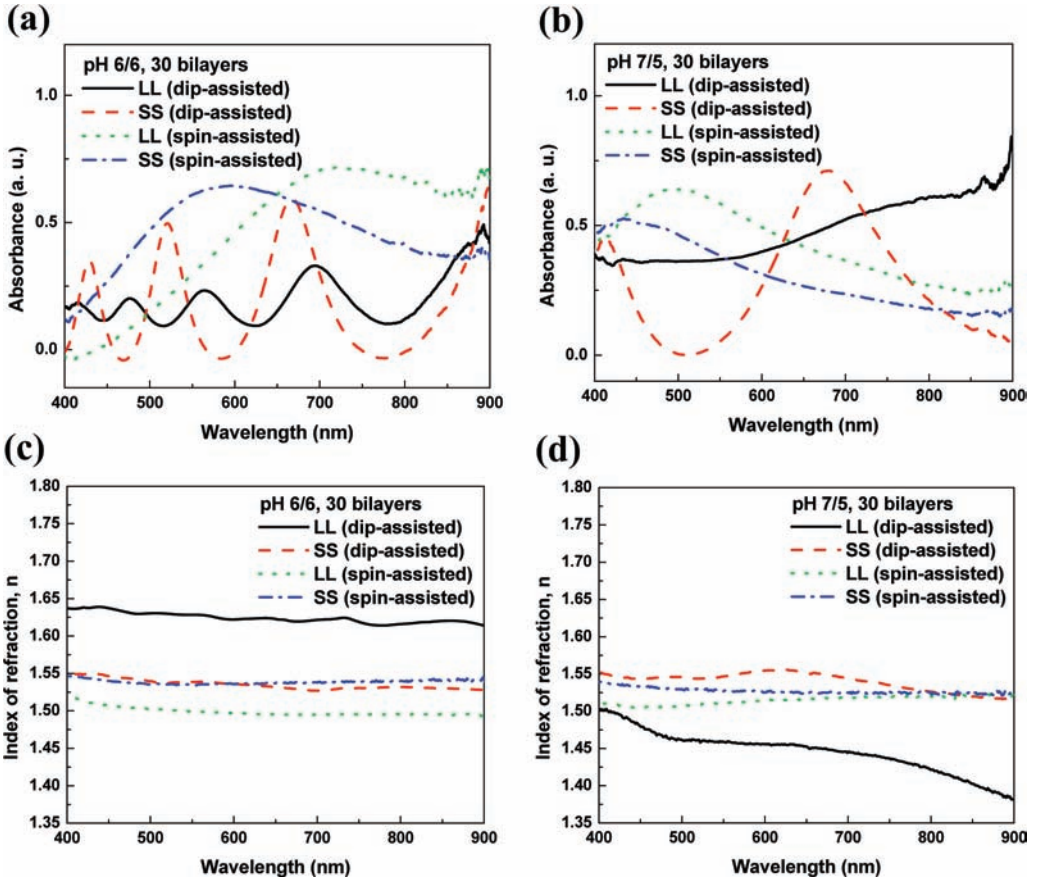

Figure 6. UV−vis spectra in a reflective mode (a and b) and index of refraction (c and d) for LbL multilayer films with 30 bilayers prepared at different deposition pH pairs: pH 6/6 (a and c) and pH 7/5 (b and d).

dx.doi.org/10.1021/ja203106c |J. Am. Chem. Soc. 2011, 133, 9592–9606

and AFM microscopies (Table 3). Apparently, the thickness of the LbL film has widespread local uniformity over large surface areas with regions of uniform thicknesses of a few micrometers across despite the surface corrugations. These large surface regions act as coherent domains not causing excessive light scattering in the visible range in contrast to most exponentially grown thick films. In fact, such an optical uniformity is a rare observation for exponentially grown LbL films, which usually become opaque quickly with a growing number of layers due to the intense microphase separation and increased roughness on a sub-micrometer level. Remarkably, the estimation of the thickness of the LbL films from analyzing different orders of interference gives thicknesses which are close to independent AFM and ellipsometry measurements (Table 3).[96] This close correspondence confirms the true nature of the rich colors produced as coming from large microscopic domains with extremely uniform thickness over large surface areas.

Finally, the ellipsometry measurements of LbL films show refractive indices within a range of 1.52−1.63 for longer wavelengths (Figure 6). The significant decrease in the effective refractive index for linear/linear LbL films from 1.63 at pH 6/6 to 1.45 at pH 7/5 is caused by the formation of laterally nonuniform films due to microphase separation. However, all other LbL films show virtually unchanged refractive indices indicating that pH-triggered reorganizations do not result in significant changes in material properties.

Exponential Growth for Different Star Architectures. To examine the effect of polymer components with different architectures on the exponential growth mode, linear/star pairs were further investigated at pH 6/6 and pH 7/5 (Table 2, Figure 7). Thicker LbL films display a linear buildup over a wide range from 9 to 30 bilayers, which can be described as $d = An + B$, where d is the thickness, n is the number of bilayers, A is the slope corresponding to the thickness of one bilayer, and B is the d-intercept (Figure 7a). The rate of growth in the linear mode is similar for all LbL films with an around 100 nm/bilayer. Such extremely large growth rates in a linear mode indicate a significant dependence of component diffusion during polyelectrolyte deposition on the amount of material deposited during a single step, which seems to have far exceeded the expected value for single monolayers of polyelectrolytes in nondisturbed conformations.

The exponential growth mode was analyzed by using the known equation: $d = A_0 e^{n/\tau}$, where d denotes thickness, A_0 is a scaling parameter, n is the number of bilayers, and τ corresponds to the characteristic growth time (Table 4).[62,97,98] Such an analysis shows that the growth mode for all polymer pairs is described by the exponential model with $R^2 \sim 0.98$ (Figure 7b). The linear/linear pairs show the highest growth rate while the star/star pairs possess the slowest rate of exponential growth. The linear/star combinatory pairs lie between the growth rates of linear/linear and star/star pairs. The overall characteristic growth parameter τ for LbL films studied here is within 1.2−1.5 for pH 6/6 and 2.2−3.0 for pH 7/5 (Table 4). These parameters indicate that the rate of exponential growth for pH 7/5 conditions is similar to those reported earlier for various LbL films (usually within 2−3).[62,92] In contrast, at pH 6/6 a much higher (twice) rate of exponential growth (two times lower τ) is observed for all component combinations studied here (Table 4).

In contrast to pH 6/6, at pH 7/5 exponential growth occurs for all linear and star pairs studied here after a period of slow growth during the initial few depositions (Figure 7c).

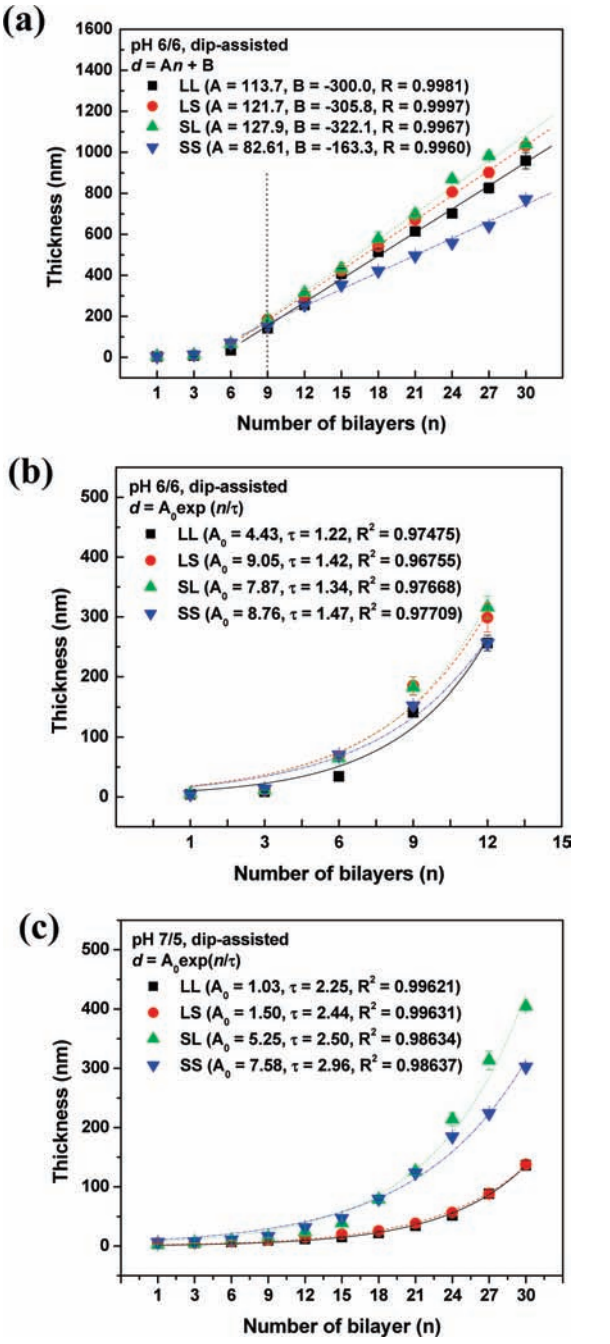

Figure 7. Buildup curve of the LbL multilayer films assembled with varying chain topology as a function of the number of bilayers assembled by the dip-assisting method at different pH conditions of pH 6/6 (a and b) and pH 7/5 (c): LL (■), LS (●), SL (▲), and SS (▼). (a) The linear growth curve is obtained by fitting data in the linear buildup region (n = 9−30) into a function of $d = An + B$ for pH 6/6. (b) The exponential growth rate is obtained by fitting the data into a function of $d = A_0 \exp(n/\tau)$ (n = 1−12) for pH 6/6 (b) and (n = 1−30) for pH 7/5 (c).

Exponential analysis shows excellent fit with R^2 = 0.99 throughout the whole range of n from 1 to 30 bilayers (Figure 7c, Table 4). Comparison of different assembling conditions reveals an overall lower rate of growth at 7/5 as compared to that at pH 6/6 (Table 4). Such a difference can be related to the stronger intermolecular interactions at pH 7/5 than pH 6/6. The

dx.doi.org/10.1021/ja203106c |J. Am. Chem. Soc. 2011, 133, 9592–9606

increased degree of ionic cross-linking can lead to the suppressed diffusion of polymer within LbL films. Also, the flat and smooth surface morphology due to the further extended conformation at pH 7/5 seems to contribute to the lower exponential growth.

A summary of the morphological parameters (terminal thickness for 30 bilayers and large-scale roughness on the scale of 10 μm × 10 μm) for all four polyelectrolyte pairs is presented in Figure 8, and corresponding AFM images are displayed in Figure 9. As apparent from these data, exponentially grown linear/linear p(AA)/p(DMAEMA) LbL films possess the most nonuniform morphology with large-scale microphase separation, resulting in excessive roughness of about 50 nm on the scale

Table 4. Exponential Growth Rate Parameters for Dip-Assisted LbL [a]

pH	polymer pair	τ	A_0
6/6	LL	1.22	4.43
	LS	1.42	9.05
	SL	1.34	7.87
	SS	1.47	8.76
7/5	LL	2.25	1.03
	LS	2.44	1.50
	SL	2.50	5.25
	SS	2.96	7.58

[a] All results were obtained by fitting the thickness data versus the number of bilayers into the exponential growth formula represented by $d = A_0 e^{n/\tau}$ (d denotes the thickness of the LbL film, and n is the number of bilayers).

10 μm × 10 μm for both assembly conditions. Similar morphological features are observed for star/linear pairs with the high surface roughness for these pairs reaching 40 nm on the scale of 10 μm × 10 μm (Figure 8). Such a difference for star-containing LbL films suggests that the linear components contribute to the exponential growth via surface roughening due to the faster diffusion and higher mobility caused by weak ionic interactions of the p(AA) or p(DMAEMA) chains.

In striking contrast, all star-containing LbL films show consistent exponential growth with the formation of thick and smooth films with surface roughnesses on the 10 μm × 10 μm scale not exceeding 2.0 nm for pH 6/6, a small value for LbL films (Figure 8). This value increases only modestly to 5−15 nm at pH 7/5 deposition conditions.

Moreover, higher resolution AFM images show near uniform morphology at a sub-micrometer scale with a modest aggregation of components with the formation of network morphology with a mesh size of 100−200 nm (Figure 9; note that the AFM images for pH 7/5 are presented at two different Z-scales to show all details of the rich surface morphology at different spatial scales).

These distinct and uniform morphologies, which do not occur in rough and microphase-separated exponentially grown linear/linear LbL films, might be attributed to the combination of high interdiffusion of star polyelectrolytes through the swollen matrix due to lower ionic cross-linking and a weak degree of ionization.

Shear Rates and Resulting Spin-Assisted LbL Morphologies. To probe the LbL assembly behavior under variable shear force, we studied the surface morphology of linear/linear and star/star pairs under selected conditions at increasing intervals of the rotational velocity up to 8000 rpm during spin-assisted deposition. Figure 10 presents the thickness increase for these LbL films

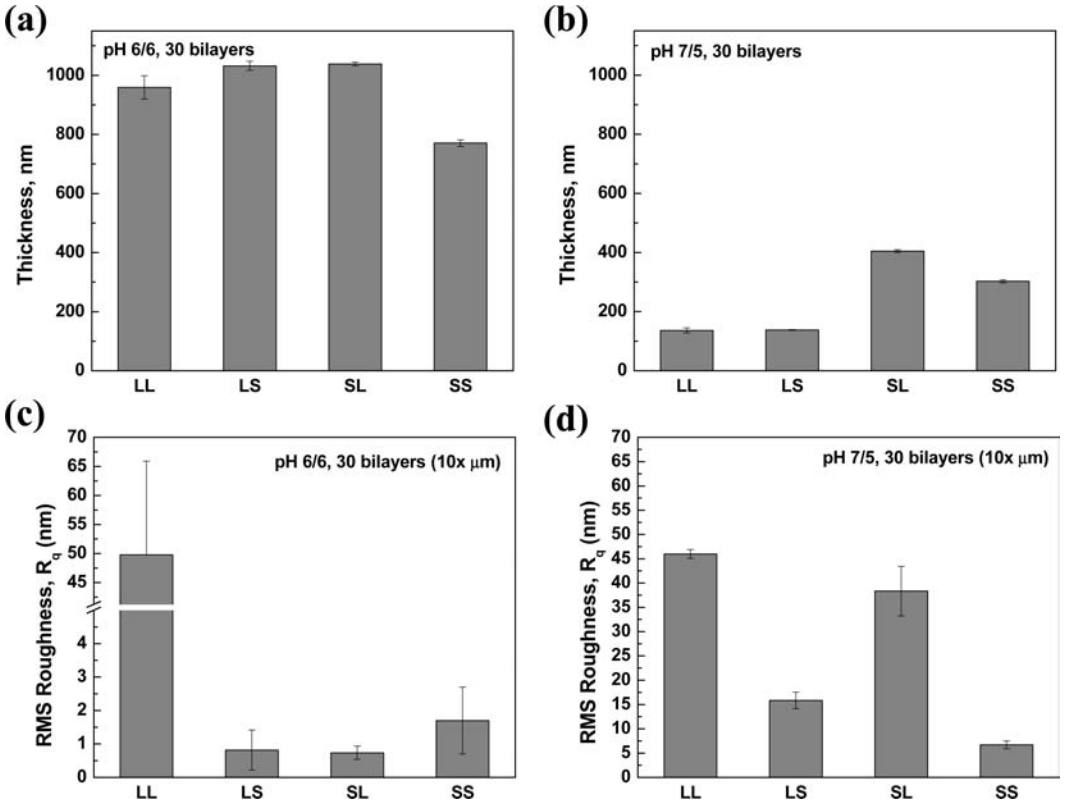

Figure 8. Variations of thickness (a and b) and RMS roughness (R_q) (c and d) of the 30 bilayered dip-assisted LbL films for different polymer pairs at pH 6/6 (a and c) and pH 7/5 (b and d).

dx.doi.org/10.1021/ja203106c | J. Am. Chem. Soc. 2011, 133, 9592–9606

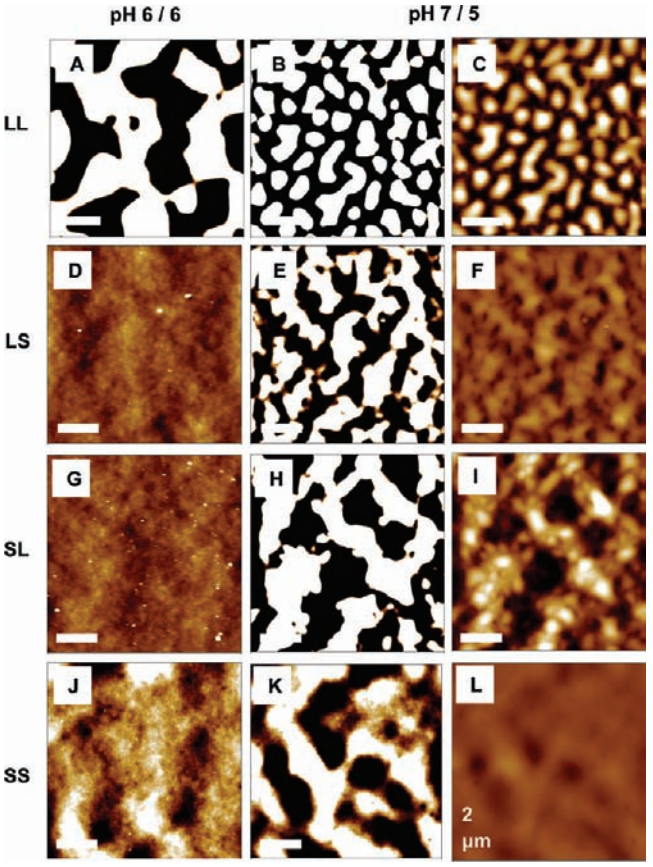

Figure 9. AFM topography images of the LbL multilayer films with different polymer pairs assembled at pH 6/6 (A−J, left) and pH 7/5 (B−K, middle and C−L, right) using the dip-assisted method: LL (A−C), LS (D−F), SL (G−I), and SS (J−L). The scale bar is 2 μm, and the *Z* scale is 10 nm for all images; and the *Z* scale is 10 nm (A−J, left and B−K, middle) and 200 nm (C−L, right).

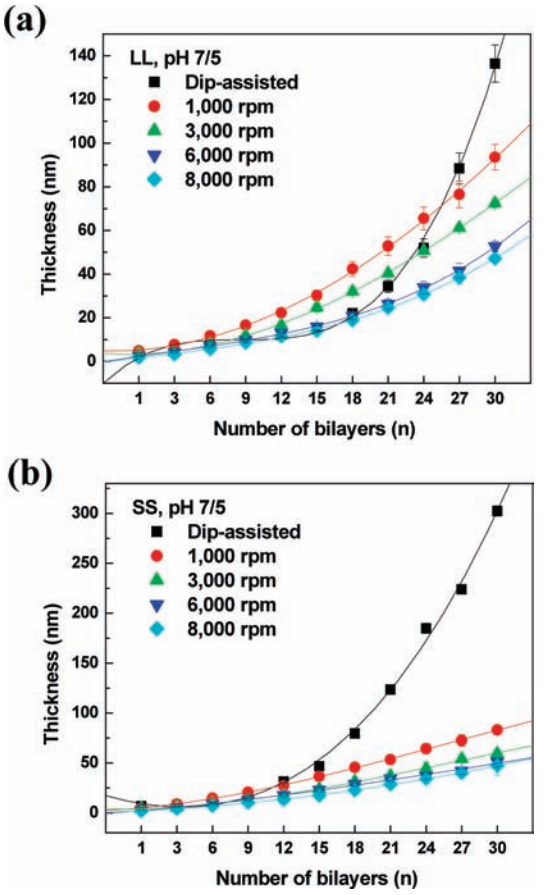

Figure 10. Buildup curve of the LbL films fabricated with dip- and spin-assisted methods for LL (a) and SS (b) polymer pairs at different spinning speeds in the range of 0−8000 rpm at pH 7/5 (the lines are a guide to the eye).

at 0 (dip-assisted), 1000, 3000, 6000, and 8000 rpm. For all spin-assisted LbL films shown here, the growth profiles is near-linear or slow exponential growth for both linear/linear and star/star pairs in contrast to the fast exponential growth observed for dip-assisted LbL films.

Overall, the resulting spin-assisted LbL films are 2−6 times thinner than their dip-assisted counterparts. This behavior is in sharp contrast to that observed for other LbL components such as p(SS) and p(AH) with much thicker films built via spin-assisted LbL assembly.[84] Such difference can be caused by the much weaker interactions between p(AA) and p(DMAEAMA) components under given pH conditions and the suppressed interdiffusion during spin-assisted LbL assembly.

It is also interesting that although dip-assisted LbL films from star/star pairs are much (twice) thicker than that from linear/linear pairs, the same star/star films prepared with spin-assisted LbL assembly are much (up to 50%) thinner (Figure 10). Such a dramatic thinning of the star/star LbL films under intense shearing could be related to the fact that star polyelectrolytes retain their more compact shape and higher mobility in fluidic flow. Both contributions should result in a reduced amount of material tethered to the substrate in the course of spin-casting. This effect is confirmed by the strong role of the increasing shear rates with the thinnest LbL films obtained at the highest rotational velocities (Figure 10).

To elucidate the true nature of structural changes occurring during spin-assisted assembly, AFM measurements were taken to examine the surface morphology versus the shear rate for these LbL films (Supporting Information Figure S6). As was discussed above, the surface morphology of dip-assisted linear/linear LbL films is nonuniform with microscopic irregular surface domains and a wormlike morphology with high roughness reaching 45 nm for the 10 μm × 10 μm surface area (Figure S6a). In contrast, star/star LbL film show a more uniform morphology with some larger-scale surface corrugations, occasional holes, and much lower overall roughness of 7.0 nm on the scale of 10 μm × 10 μm. The presence of holes may be attributed to either insufficient coverage or traces of draining solvent or air bubbles trapped within the multilayer film, which were not removed during the assembly process.

On the other hand, spin-casting of both linear and star polyelectrolytes results in a much smoother surface morphology with a dramatically reduced roughness below 2.0 nm and a thickness down to 30−50 nm on the 10 μm × 10 μm (Figures S6 and S7). Such thinning and smoothing can be related to the removal of larger, weakly tethered aggregates clearly visible for LbL films obtained by the dip-assisted method and a suppression of lateral diffusion/microphase separation of components during fast (a fraction of a second) removal of solvent. Moreover, a further increase in the shear rate results in the progression of this reorganization with a gradually decreased film thickness and increased

dx.doi.org/10.1021/ja203106c |*J. Am. Chem. Soc.* 2011, 133, 9592–9606

Scheme 2. Model Structure of LbL Multilayer Films Displaying the Surface Structure and Expected Molecular Organization within the LbL Assemblies: (a) Spin-Assisted LbL for Star and (b) Dip-Assisted LbL for Linear (Top) and Star (Bottom) Polymer at Different pH Conditions of pH 6/6 (Left) and pH 7/5 (Right)[a]

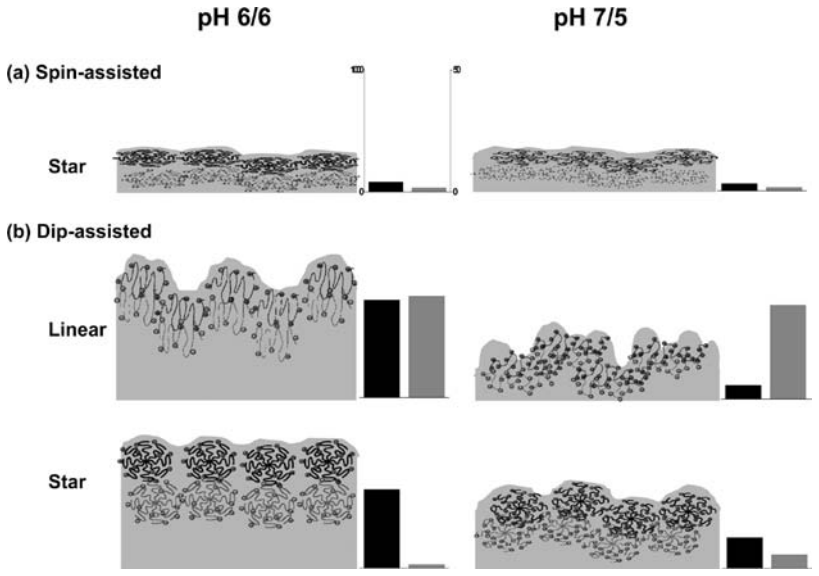

[a] Gray-colored boxes represent the LbL films with different thicknesses and surface roughness, but their values are not set to the same length scale for all drawings. The histograms on the right hand side of each drawing show the average thickness (black, left) and roughness (gray, right) with the left *y*-axis (1000 nm) for thickness and right *y*-axis (50 nm) for roughness for 30 bilayer LbL films. The bar graphs are all on the same scale.

roughness on the scale of 10 μm × 10 μm and domain size for both linear/linear and star/star polyelectrolytes (Figures S6 and S7).

GENERAL DISCUSSION AND CONCLUSIONS

The assembly behavior, growth modes, and surface morphologies of LbL films composed of cationic p(DMAEMA) and anionic p(AA) weak polyelectrolyte stars at different deposition pH conditions close to the pK_a of the star polyelectrolytes (pK_a ∼ 5.8 and 6.7 for respective components) were found to be critically dependent on the interplay of intermolecular interactions and conformational states, as will be discussed in this section.

First, we will discuss different modes of growth of the LbL films assembled with spin-assisted and dip-assisted routines. As we observed here, the spin-assisted method results in the stable and linear growth of LbL films from any combination of star and linear counterparts under all pH and shearing conditions tested here. The characteristic feature of this growth mechanism is the low rate of growth of 2−4 nm/bilayer. This growth rate is many times smaller than the unperturbed dimensions of the polymer chains exploited here (10−30 nm), indicating that both star and linear polyelectrolyte components become highly flattened and compacted with excessive material removal under strong shearing forces and fast solvent removal.

The significant decrease in bilayer thicknesses observed here for spin-assisted LbL films is in striking contrast to that reported for conventional linear strong polyelectrolytes, which show much thicker spin-assisted LbL films obtained as compared to dip-assisted LbL films.[53,56] In the case of the strong polyelectrolytes studied earlier, the increased thickness was associated with a higher grafting density caused by enhanced attractive interactions between oppositely charged polymer chains and very limited intermixing as was confirmed by neutron reflectivity of LbL films with deuterated components.[56] A similar phenomenon of the thinning of spin-assisted LbL films observed for p(EO) and p(AA) components was related to the suppression of the formation of a micellar morphology. The critical role of weak interactions in significant thinning was also demonstrated for short-range hydrogen-bonded spin-assisted LbL films.[99] Accordingly, the dramatic thinning of polyelectrolyte bilayers for weak polyelectrolytes studied in a pH range close to the isoelectric points of all components can be caused by weak interfacial interactions resulting in easy displacement of the adsorbed macromolecules by the fast removal of solvent and the strong shearing of polymer chains.

In fact, as has been suggested for branched, dendritic macromolecules, a full range of shapes from highly spread to pancake-like, to near-globular can be observed depending upon the strength of interfacial interactions and the type of surface assembly (grafting, Langmuir monolayers, or LbL films).[47,100−105] Indeed, star/star polymer pairs were demonstrated to show a decreased extent of entanglement and limited molecular interdiffusion due to the compact and globular structure of branched molecules.[79] However, dendritic and hyperbranched macromolecules usually possess uniform chemical composition and surface-bonded functionalities. The occurrence of microphase separation of different long-chain arms within multiarm star block copolymers and uniform ion distribution across loosely packed star block copolymers are the most critical factors affecting their assembly behavior.

Apparently, the attachment of polycationic and polyanionic chains to a single, but relatively voluminous, core in star polymers does not significantly affect the resulting morphology of spin-assisted LbL films. Virtually identical thicknesses and surface morphologies of LbL films for all linear/linear, linear/star, and star/star polyelectrolyte pairs suggest that, under low grafting density conditions, architectural confinement does not affect the ability of relatively long, flexible, and weakly charged arms to adapt a highly flattened, pancakelike conformation (Scheme 2).

Histograms with actual film thicknesses and microroughnesses which are placed next to the film schematics clearly quantify and scale dramatic changes in the LbL film morphologies for different compositions and different pH assembling conditions.

The overall morphology of spin-assisted LbL films remains stable over a wide range of assembling conditions within a range of pH 5−7, which can be related to the modest variation of macromolecular dimensions and degree of ionization. This is especially true for star polyelectrolytes in contrast to the dramatic changes usually observed for linear polyelectrolytes within a narrow pH range.[31,106] Therefore, this growth behavior supports the suggestion that the star structure limits the chain entanglements due to steric hindrance and, as a result, suppresses the ionic cross-linking and reduces adherence to the substrate.

In contrast to spin-assisted LbL films, the corresponding dip-assisted LbL films fabricated from star and linear p(DMAEMA) and anionic p(AA) show a rich pattern of different exponential growth modes controlled by the preparation conditions and molecular architecture (Scheme 2). Apparently, the dip-assisted environment with a long time available for swelling and interaction with solution is kinetically more favorable for extensive interdiffusion of components, large-scale molecular aggregation, and lateral diffusion of aggregates.

The first and most crucial conclusion is that weak star polyelectrolytes are capable of growing thick LbL films in an exponential growth mode. This result is even more surprising considering that star polyelectrolytes with high molecular weight and a large number of arms have been observed to be capable of growing only in the linear mode due to slow diffusion of star polyelectrolytes that prevents the common diffusion mechanism of fast exponential growth. Moreover, to date, only rough and thin LbL films have been fabricated via a linear growth mode with a small increment per bilayer (within 1−8 nm) with a few exceptions discussed below.[78,79] In contrast, the star/star and star/linear LbL assemblies studied here demonstrate an exponential growth mode with an increment per bilayer reaching 100 nm with differences in significant roughening.

The analysis of the experimental data with a generalized exponential function shows excellent correspondence of the growth kinetics to an extended slow growth phase and an exponential growth up to a very large number of bilayers (up to 30) in the case of the pH 7/5 LbL assemblies (Figure 7, Table 4). At milder pH 6/6 conditions, close to the pK_a for both components, the LbL growth becomes even more dramatic with a narrow slow growth phase for the first few bilayers and then enters a fast exponential growth regime for n = 5−15, followed by linear growth for n = 15−30 (Figure 7). As a result, the LbL film reached 1 μm thickness which is many times higher than that for a dip-assisted LbL film fabricated earlier for star-based LbL films with an even higher molecular weight of components (30−80 nm for n = 10−16).[78,79]

At the pH 6/6 assembly condition, the rates of growth of star/star and linear/linear LbL films are similar although the total effective "molecular weight" of a bilayer of a stoichiometric composition is much lower for the linear/linear pair (239 000 vs 680 000 g/mol) (Table 1). This effect suggests a more compact shape of star polyelectrolytes (per unit of mass) and probably less efficient uptake of star polyelectrolytes with much lower specific charge density per unit of volume during the buildup of LbL assemblies. On the other hand, the rate of growth at pH 7/5 is the highest for star/star LbL films with twice higher thickness as compared to that for linear/linear pairs (Figure 7). Such a difference can be associated with the slightly increased ionic interactions of the higher charged polycationic component with a dominating molecular weight contribution.

The investigation of the exponential growth rate for different component pairs such as linear/linear, linear/star, star/linear, and star/star LbL assemblies reveals that the pH 6/6 condition gives the highest growth rate with a resulting thicker film reflecting a stronger tendency toward the diffusion of star polyelectrolyte components during exposure to oppositely charged polyelectrolytes, but without excessive roughening due to molecular aggregation caused by lateral microphase separation after the completed deposition cycle (Scheme 2). It has been known that the exponential rate depends on the molecular weight and the mismatch in molecular size and ionic charge density.[62,61] These higher growth rates seem to be consistent with the lower ionic cross-link density of star polyelectrolytes at pH 6/6, thereby suggesting the weak ionic density is critical for the facilitation of an exponential growth mode even for the high molecular weight star polyelectrolytes employed in this study. That is, the larger number of "loosely complexed" polymer chains at pH 6/6 could effectively contribute to the complexation because of mismatched ionic charges.[62,74,92] The retarded exponential buildup at the initial stages at pH 7/5 can be explained by the higher ionic density and lower molecular weight of linear/linear and linear/star pairs than that for star/linear and star/star pairs. The compact branched architecture of the star polymer would limit the ionic complexation mainly in the outer shell, which might lead to large mismatching in ionic pairing. Thus, effective ionic charges that can contribute to ionic cross-linking may be lower than that for the linear counterpart, which might allow for high mobility within LbL films and facilitate the exponential growth of all star LbL films, a unique finding of this study.

However, the lower ionic density and higher ionic state mismatch between polyanionic and polycationic components at pH 6/6, particularly when incorporating the star component, lead to thicker and more uniform LbL films. Notably, the resulting morphology of exponentially grown star-containing LbL films is different from similar linear/linear pairs. The linear/linear pairs show well-developed "wormlike" surface morphology with large surface roughness on the 10 μm × 10 μm. For star component containing LbL films the isolated and partially interconnected domain network appears to transform to a fully interconnected large-scale wormlike morphology which is, however, underpinned with a thicker material film. We suggest that the increased mass adsorption at pH 6/6 as well as the higher mobility of star polymer chains due to lower ionic density could lead to both a higher adsorption rate during the deposition step and, as a result, a reduced lateral aggregation due to the slow diffusion of star complexes.[73,74] This appears due to a combination of fast interdiffusion of components and their complexes followed by lateral microphase separation of dissimilar components and their complexes (Scheme 2).[48,59,62,74,75] The dramatically increased surface roughness enhances accelerated film buildup due to increased specific interfacial area and a higher probability of the interfacial adsorption during sequential exposure to solutions.[78,107] This model seems validated for linear/linear pairs of linear components, anionic p(AA) and cationic p(DMAEMA), by all experimental data acquired here.

It is important to note that to date very few studies attempted to exploit star polyelectrolyte for LbL assembly with a very limited selection of linear and star components and for a limited number of bilayers (below 10). In these studies, either the

traditional linear growth mode was observed and associated with slow diffusion of high molecular weight star polyelectrolyte[79] or some evidence of the exponential growth has been noticed for a few limited cases.[78,80] In contrast, in this study we introduced a far more comprehensive combination of linear and star polyelectrolyte components with a wide range of molecular architectures and assembling conditions covering critical pH combinations and an extended number of assembling cycles (up to 60). Such a comprehensive analysis unexpectedly revealed a uniquely rich LbL assembling behavior and morphologies of star polyelectrolytes with an extended combination of all linear, exponential, and linear/exponential modes of growth to be controlled by pH conditions and component nature.

In fact, we observed that the exponential growth of linear/linear pairs results in a rough (>50 nm roughness on the 10 μm × 10 μm) wormlike morphology caused by intense microphase aggregation of components, whereas the star/star LbL films from chemically identical polyelectrolyte components undergo very different growth mechanism. For star/star polyelectrolyte pairs thick, uniform, and molecularly smooth exponentially grown LbL films have been revealed in this study. We suggest that star polyelectrolytes with compact shape, partially screened charges, and high diffusion mobility facilitate fast complexation and lead to exponential buildup of the LbL films. This fast buildup is likely to hinder efficient lateral diffusion of components and thus prevents large-scale microphase separation, which results in smooth, locally uniform, thick, and optically transparent LbL films with rich interference properties, a unique combination for exponentially grown LbL films from traditional linear polyelectrolytes.

■ ASSOCIATED CONTENT

Supporting Information. Table S1 listing the thickness and roughness of LS LbL films and Figures S1−S7 showing polarized angles and phases of LbL multilayer films, AFM topography images, contact angle, optical microscopy images, and variations of thickness and RMS roughness. This information is available free of charge via the Internet at http://pubs.acs.org/.

■ AUTHOR INFORMATION

Corresponding Author
vladimir@mse.gatech.edu

Present Addresses
[§]Institute of Physical Chemistry, RWTH Aachen University, Landoltweg 2, 52056 Aachen, Germany.

■ ACKNOWLEDGMENT

This work is supported by the NSF-DMR 1002810 grant and the Department of Energy DE-SC0002232 grant. C.V.S. gratefully acknowledges funding by the state of Bavaria through the BayEFG and support by the Elite Network of Bavaria (ENB). The authors thank Z. Combs for technical assistance. V.V.T. thanks Humboldt Foundation for support.

■ REFERENCES

(1) Decher, G. *Science* **1997**, *277*, 1232–1237.
(2) Decher, G.; Schlenoff, J. B.; Lehn, J.-M. *Multilayer Thin Films: Sequential Assembly of Nanocomposite Materials*; Wiley-VCH: Weinheim, Germany, 2003; pp 1−524.
(3) Lvov, Y.; Decher, G.; Möhwald, H. *Langmuir* **1993**, *9*, 481–486.
(4) Lvov, Y.; Möhwald, H. *Protein Architecture: Interfacial Molecular Assembly and Immobilization Biotechnology*; Dekker: New York, 2000; pp 1−394.
(5) Mamedov, A. A.; Kotov, N. A. *Langmuir* **2000**, *16*, 5530–5533.
(6) Chen, K. M.; Jiang, X.; Kimerling, L. C.; Hammond, P. T. *Langmuir* **2000**, *16*, 7825–7834.
(7) Mendelson, J. D.; Barret, C. J.; Chan, V. V.; Pal, A. J.; Mayes, A. M.; Rubner, M. F. *Langmuir* **2000**, *16*, 5017–5023.
(8) Caruso, F.; Susha, A. S.; Giersig, M.; Mohwald, H. *Adv. Mater.* **1999**, *11*, 950–953.
(9) Swiston, A. J.; Cheng, C.; Um., S. H.; Irvine, D. J.; Cohen, R. E.; Rubner, M. F. *Nano Lett.* **2008**, *8*, 4446–4453.
(10) Hammond, P. T. *Adv. Mater.* **2004**, *16*, 1271–1293.
(11) Jiang, C.; Tsukruk, V. V. *Soft Matter* **2005**, *1*, 334–337.
(12) Jaber, J. A.; Schlenoff, J. B. *Curr. Opin. Colloid Interface Sci.* **2006**, *11*, 324–329.
(13) Nolte, M.; Schoeler, B.; Peyratout, C. S.; Kurth, D. G.; Fery, A. *Adv. Mater.* **2005**, *17*, 1665–1669.
(14) Sukhishvili, S. A. *Curr. Opin. Colloid Interface Sci.* **2005**, *10*, 37–44.
(15) Ariga, K.; Ji, Q.; Hill, J. P. *Adv. Polym. Sci.* **2010**, *229*, 51–87.
(16) Zhai, L.; Nolte, A. J.; Cohen, R. E.; Rubner, M. F. *Macromolecules* **2004**, *37*, 6113–6123.
(17) Kozlovskaya, V.; Harbaugh, S.; Drachuk, I.; Shchepelina, O.; Kelley-Loughnane, N.; Stone, M.; Tsukruk, V. V. *Soft Matter.* **2011**, *7*, 2364–2372.
(18) Kharlampieva, E.; Sukhishvili, S. A. *Polymer Rev.* **2006**, *46*, 377–395.
(19) Kotov, N. A. *Nanostruct. Mater.* **1999**, *12*, 789–796.
(20) Dubas, S.; Schlenoff, J. B. *Macromolecules* **1999**, *32*, 8153–8160.
(21) Luzinov, I.; Minko, S.; Tsukruk, V. V. *Prog. Polym. Sci.* **2004**, *29*, 635–698.
(22) Stuart, M. A. C.; Huck, W. T. S.; J., G.; Müller, M.; Ober, C.; Stamm, M.; Sukhoruko, G. B.; Szleifer, I.; Tsukruk, V. V.; Urban, M.; Winnik, F.; Zauscher, S.; Luzinov, I.; Minko, S. *Nat. Mater.* **2010**, *9*, 101–113.
(23) Kozlovskaya, V.; Kharlampieva, E.; Khanal, B. P.; Manna, P.; Zubarev, E. R.; Tsukruk, V. V. *Chem. Mater.* **2008**, *20*, 7474–7485.
(24) Kozlovskaya, V.; Kharlampieva, E.; Drachuk, I.; Cheng, D.; Tsukruk, V. V. *Soft Matter* **2010**, *6*, 3596–3608.
(25) Lavalle, P.; Voegel, J.-C.; Vautier, D.; Senger, B.; Schaaf, P.; Ball, V. *Adv. Mater.* **2011**, *23*, 1191–1221.
(26) Wilson, J. T.; Cui, W.; Kozlovskaya, V.; Kharlampieva, E.; Pan, D.; Qu, Z.; Krishnamurthy, V. R.; Mets, J.; Kumar, V.; Wen, J.; Song, Y.; Tsukruk, V. V.; Chaikof, E. L. *J. Am. Chem. Soc.* **2011**, *133*, 7054–7064.
(27) Caruso, F. *Adv. Mater.* **2001**, *13*, 11–22.
(28) Kharlampieva, E.; Sukhishvili, S. A. *Langmuir* **2003**, *19*, 1238–1243.
(29) Choi, J.; Rubner, M. F. *Macromolecules* **2005**, *38*, 116–124.
(30) Itano, K.; Choi, J.; Rubner, M. F. *Macromolecules* **2005**, *38*, 3450–3460.
(31) Philippova, O. E.; Hourdet, D.; Audebert, R.; Khokhlov, A. R. *Macromolecules* **1997**, *30*, 8278–8285.
(32) Jiang, C.; Tsukruk, V. V. *Adv. Mater.* **2006**, *18*, 829–840.
(33) Wang, J. S.; Matyjaszewski, K. *J. Am. Chem. Soc.* **1995**, *117*, 5614–5615.
(34) Matyjaszewski, K.; Xia, J. *Chem. Rev.* **2001**, *101*, 2921–2990.
(35) Plamper, F.; Becker, H.; Lanzendorfer, M.; Patel, M.; Wittemann, A.; Ballauff, M.; Müller, A. H. E. *Macromol. Chem. Phys.* **2005**, *206*, 1813–1825.
(36) Muthukrishnan, S.; Plamper, F.; Mori, H.; Müller, A. H. E. *Macromolecules* **2005**, *38*, 10631–10642.
(37) Plamper, F. A.; McKee, J. R.; Laukkanen, A.; Nykänen, A.; Walther, A.; Ruokolainen, J.; Aseyev, V.; Tenhu, H. *Soft Matter* **2009**, *5*, 1812–1821.
(38) Plamper, F. A.; Murtomäki, L.; Walther, A.; Kontturi, K.; Tenhu, H. *Macromolecules* **2009**, *42*, 7254–7257.

(39) Plamper, F. A.; Reinicke, S.; Elomaa, M.; Schmalz, H.; Tenhu, H. *Macromolecules* **2010**, *43*, 2190–2203.
(40) Peleshanko, S.; Gunawidjaja, R.; Jeong, J.; Shevchenko, V. V.; Tsukruk, V. V. *Langmuir* **2004**, *20*, 9423–9427.
(41) Pelschanko, S.; Jeong, J.; Gunawidjaja, R.; Tsukruk, V. V. *Macromolecules* **2004**, *37*, 6511–6522.
(42) Gunawidjaja, R.; Peleshanko, S.; Tsukruk, V. V. *Macromolecules* **2005**, *38*, 8765–8774.
(43) Genson, K. L.; Hoffman, J.; Teng, J.; Zubarev, E. R.; Vaknin, D.; Tsukruk, V. V. *Langmuir* **2004**, *20*, 9044–9052.
(44) Gunawidjaja, R.; Peleshanko, S.; Kirsten, L. G.; Tsitsilianis, C.; Tsukruk, V. V. *Langmuir* **2006**, *22*, 6168–6176.
(45) Tsukruk, V. V. *Prog. Polym. Sci.* **1997**, *22*, 247–311.
(46) Nguyen, P. M.; Zacharia, N. S.; Verploegen, E.; Hammond, P. T. *Chem. Mater.* **2007**, *19*, 5524–5530.
(47) Tsukruk, V. V. *Adv. Mater.* **1998**, *10*, 253–257.
(48) Zacharia, N. S.; Modestino, M.; Hammond, P. T. *Macromolecules* **2007**, *40*, 9523–9528.
(49) Zacharia, N. S.; Delongchamp, D. M.; Modestino, M.; Hammond, P. T. *Macromolecules* **2007**, *40*, 1598–1603.
(50) Plamper, F. A.; Schmalz, A.; Penott-Chang, E.; Drechsler, M.; Jusufi, A.; Ballauff, M.; Müller, A. H. E. *Macromolecules* **2007**, *40*, 5689–5697.
(51) Plamper, F. A.; Walter, A.; Müller, A. H. E.; Ballauf, M. *Nano Lett.* **2007**, *7*, 167–171.
(52) Schlenoff, J. B.; Dubas, S. T.; Farhat, T. *Langmuir* **2000**, *16*, 9968–9969.
(53) Cho, J.; Char, K.; Hong, J.-D.; Lee, K.-B. *Adv. Mater.* **2001**, *13*, 1076–1078.
(54) Cho, J.; Lee, S.-H.; Kang, H.; Char, K.; Koo, J.; Byoung, H. S.; Lee, K.-B. *Polymer* **2003**, *44*, 5455–5459.
(55) Jiang, C.; Markutsya, S.; Tsukruk, V. V. *Langmuir* **2004**, *20*, 882–890.
(56) Jiang, C.; Markutsya, S.; Tsukruk, V. V. *Adv. Mater.* **2004**, *16*, 157–161.
(57) Schoeler, B.; Poptoshev, E.; Caruso, F. *Macromolecules* **2003**, *36*, 5253–5264.
(58) Salomaki, M.; Vinokurov, I. A.; Kankare, J. *Langmuir* **2005**, *21*, 11232–11240.
(59) Laugel, N.; Betscha, C.; Winterhalter, M.; Voegel, J.-C.; Schaaf, P.; Ball, V. *J. Phys. Chem. B* **2006**, *110*, 19443–19449.
(60) Porcel, C.; Lavalle, P.; Decher, G.; Senger, B.; Voegel, J.-C.; Schaaf, P. *Langmuir* **2007**, *23*, 1898–1904.
(61) Sun, B.; Jewell, C. M.; Fredin, N. J.; Lynn, D. M. *Langmuir* **2007**, *23*, 8452–8459.
(62) Jiang, C.; Ko, H.; Tsukruk, V. V. *Adv. Mater.* **2005**, *17*, 2127–2131.
(63) Jiang, C.; Markutsya, S.; Shulha, H.; Tsukruk, V. V. *Adv. Mater.* **2005**, *17*, 1669–1673.
(64) Zimnitsky, D.; Shevchenko, V. V.; Tsukruk, V. V. *Langmuir.* **2008**, *24*, 5996–6006.
(65) Jiang, C.; Wang, X.; Gunawidjaja, R.; Lin, Y.-H.; Gupta, M. K.; Kaplan, D. L.; Naik, R. R.; Tsukruk, V. V. *Adv. Funct. Mater.* **2007**, *17*, 2229–2237.
(66) Kozlovskaya, V.; Kharlampieva, E.; Jones, K.; Lin, Z.; Tsukruk, V. V. *Langmuir* **2010**, *26*, 7138–7147.
(67) Kujawa, P.; Moraille, P.; Sanchez, J.; Badia, A.; Winnik, F. M. *J. Am. Chem. Soc.* **2005**, *127*, 9224–9234.
(68) Kolasinska, M.; Krastev, R.; Gutberlet, T.; Warszynski, P. *Langmuir* **2009**, *25*, 1224–1232.
(69) Jiang, C.; Markutsya, S.; Pikus, Yu.; Tsukruk, V. V. *Nat. Mater.* **2004**, *3*, 721–728.
(70) Chiarelli, P. A.; Johal, M. S.; Casson, J. L.; Roberts, J. B.; Robinson, J. M.; Wang, H.-L. *Adv. Mater.* **2001**, *13*, 1167–1171.
(71) Lee, S.-S.; Hong, J.-D.; Kim, C. H.; Kim, K.; Koo, J. P.; Lee., K.-B. *Macromolecules* **2001**, *34*, 5358–5360.
(72) Elbert, D. L.; Herbert, C. B.; Hubbell, J. A. *Langmuir* **1999**, *15*, 5355–5362.
(73) Picart, C.; Lavalle, Ph.; Hubert, P.; Guisinier, F. J. G.; Decher, G.; Schaaf, P.; Voegel, J.-C. *Langmur* **2001**, *17*, 7414–7424.
(74) Lavalle, P.; Gergely, C.; Cuisinier, F. J. C.; Decher, G.; Schaaf, P.; Voegel, J. C.; Picart, C. *Macromolecules* **2002**, *35*, 4458–4465.
(75) Lavalle, P.; Picart, C.; Mutterer, J.; Gergely, C.; Reiss, H.; Voegel, J.-C.; Senger, B.; Schaaf, P. *J. Phys. Chem. B* **2004**, *108*, 635–648.
(76) Porcel, C.; Lavalle, P.; Ball, V.; Decher, G.; Senger, B.; Voegel, J.-C.; Schaaf, P. *Langmuir* **2006**, *22*, 4376–4383.
(77) Yang, S.; Zhang, Y.; Wang, L.; Hong, S.; Xu, J.; Chen, Y.; Li, C. *Langmuir* **2006**, *22*, 338–343.
(78) Connal, L. A.; Li, Q.; Quinn, J. F.; Tjipto, E.; Caruso, F.; Qiao, G. G. *Macromolecules* **2008**, *41*, 2620–2626.
(79) Kim., B.-S.; Gao, H.; Argun, A. A.; Matyjaszewski, K.; Hammond, P. T. *Macromolecules* **2009**, *42*, 368–375.
(80) Guo, Z.; Chen, X.; Xin, J.; Wu, D.; Li, J.; Xu, C. *Macromolecules* **2010**, *43*, 9087–9093.
(81) Schnitter, M.; Engelking, J.; Heise, A.; Miller, R. D.; Menzel, H. *Macromol. Chem. Phys.* **2000**, *201*, 1504–1512.
(82) Szunerits, S.; Boukherroub, R. *Langmuir* **2006**, *22*, 1660–1663.
(83) Sheller, N. B.; Petrash, S.; Foster, M. D.; Tsukruk, V. V. *Langmuir* **1998**, *14*, 4535–4544.
(84) Kharlampieva, E.; Kozlovskaya, V.; Chan, J.; Ankner, J. F.; Tsukruk, V. V. *Langmuir* **2009**, *25*, 14017–14024.
(85) Markutsya, S.; Jiang, C.; Pikus, Y.; Tsukruk, V. V. *Adv. Funct. Mater.* **2005**, *15*, 771–780.
(86) Tsukruk, V. V. *Rubber Chem. Technol.* **1997**, *70*, 430–467.
(87) McConney, M. E.; Singamaneni, S.; Tsukruk, V. V. *Polym. Rev.* **2010**, *50*, 235–286.
(88) Magonov, S. N.; Elings, V.; Whangbo, M. H. *Surf. Sci.* **1997**, *375*, L385–L391.
(89) Pincus, P. *Macromolecules* **1991**, *24*, 2912–2919.
(90) Roiter, Y.; Minko, S. *J. Am. Chem. Soc.* **2005**, *127*, 15688–15689.
(91) Yoo, D.; Shiratori, S. S.; Rubner, M. F. *Macromoelcules* **1998**, *31*, 4309–4318.
(92) Shiratori, S. S.; Rubner, M. F. *Macromolecules* **2000**, *33*, 4213–4219.
(93) Ono, S. S.; Decher, G. *Nano Lett.* **2006**, *6*, 592–598.
(94) Wong, J. E.; Zastrow, H.; Jaeger, W.; von Klitzing, R. *Langmuir* **2009**, *25*, 14061–14070.
(95) Xu, C.; Wu, T.; Drain, C. M.; Batteas, J. D.; Fasolka, M. J.; Beers, K. L. *Macromolecules* **2006**, *39*, 3359–3364.
(96) Swanepoel, R. *J. Phys. E: Sci. Instrum.* **1983**, *16*, 1214–1222.
(97) DeLongchamp, D. M.; Kastantin, M.; Hammond, P. T. *Chem. Mater.* **2003**, *15*, 1575–1586.
(98) Gu, X.; Wang, G. *Appl. Surf. Sci.* **2011**, *257*, 1952–1959.
(99) Seo, J.; Luthenhaus, J. L.; Kim, J.; Hammond, P. T.; Char, K. *Langmuir* **2008**, *24*, 7995–8000.
(100) Peleshanko, S.; Tsukruk, V. V. *Prog. Polym. Sci.* **2008**, *33*, 523–580.
(101) Mansfield, M. L. *Polymer* **1996**, *37*, 3835–3841.
(102) Tsukruk, V. V.; Rinderspacher, F.; Bliznyuk, V. N. *Langmuir* **1997**, *13*, 2171–2176.
(103) Bliznyuk, V. N.; Rinderspacher, F.; Tsukruk, V. V. *Polymer* **1998**, *39*, 5249–5252.
(104) Betley, T. A; Holl, M. M. B.; Orr, B. G.; Swanson, D. R.; Tomalia, D. A.; Baker, J. R., Jr. *Langmuir* **2001**, *17*, 2768–2773.
(105) Li, J.; Piehler, L. T.; Qin, D.; Baker, J. R.; Tomalia, D. A. *Langmuir* **2000**, *16*, 5613–5616.
(106) Laguecir, A.; Ulrich, S.; Labille, J.; Fatin-Rouge, N.; Stoll, S.; Buffle, J. *Eur. Pol. J.* **2006**, *42*, 1135–1144.
(107) Picart, C.; Mutterer, J.; Richert, L.; Luo, Y.; Prestwich, G. D.; Schaaf, P.; Voegel, J. −C.; Lavalle, P. *Proc. Natl. Acad. Sci. U.S.A.* **2002**, *99*, 12531–12535.